

High Curie Temperature for $\text{La}_{5/8}\text{Sr}_{3/8}\text{MnO}_3$ Thin Films Prepared by Pulsed Laser Deposition on Glass Substrates

M. Navasery^{1,*}, S.A. Halim^{1,*}, N.Soltani¹, G.Bahmanrokh¹, A.Dehzangi², M.Erfani H¹, A.Kamalianfar¹, S.K.Chen¹ and K.Y.Pan¹

¹Department of Physics, Science Faculty, Universiti Putra Malaysia, 43400 UPM Serdang, Selangor, Malaysia.

² Institute of Microengineering and Nanoelectronics (IMEN), Universiti Kebangsaan Malaysia, 43600 Bangi, Selangor, Malaysia.

*E-mail: navaseri@gmail.com; ahalim@science.upm.edu.my

Received: 23 August 2012 / Accepted: 22 November 2012 / Published: 1 January 2013

The manganite LSMO films were successfully grown on glass substrates without any additional buffer layer by pulsed laser deposition. The films have been investigated by X-ray diffraction (XRD), field emission-scanning electron microscope (FE-SEM), electrical and magnetic measurements. From the XRD pattern the film is found to be polycrystalline single-phase's character. The LSMO thin films growth on glass substrate, follows the island growth model with average grain size of 44.46nm. The metal-insulator transition (T_{MI}) temperature was above room temperature and electrical conduction mechanism of LSMO films below phase transition temperature (T_P) is due to the electron-electron (major) and electron-magnon scattering processes. The Curie temperature of LSMO films is around 352 K, which is one of the high T_C in all LSMO films and as our knowledge, is the highest value that is reported in literature for low cost amorphous substrates such as glass. The low resistivity, high T_{MI} and high T_C makes these LSMO films very useful for room temperature magnetic devices.

Keywords: Curie temperature, manganite, polycrystalline, pulse laser deposition.

1. INTRODUCTION

The phenomenon of colossal magnetoresistance (CMR) in perovskite manganites of $R_{1-x}A_x\text{MnO}_3$ (R=rare earth; A = divalent) have attracted much attention due to their potential applications for various devices such as field-sensor, magnetic reading heads and memories [1-3]. Most of these industrial devices are based on thin film form. Therefore, much investigation focuses on fabrication and characterization of thin films prepared by various methods. Lanthanum strontium manganites of $\text{La}_{1-x}\text{Sr}_x\text{MnO}_3$ (LSMO) with perovskite structure is a well-known material displaying colossal

magnetoresistance (CMR). This material has been intensively studied because of their high Curie temperature, large resistance change at the metal-insulator transition temperature and high degree of spin polarization of the carriers at the Fermi level. The metallic and ferromagnetic state of these manganites is usually explained by the Double-Exchange (DE) interaction between Mn^{3+} and Mn^{4+} pairs which control the magnetic and electrical properties of perovskite manganites. Pulsed Laser Deposition (PLD)[4-5] and sputtering [6] are most widely used techniques for fabrication of polycrystalline and epitaxial LSMO films. Many studies have been done to improve the quality of LSMO films such as of varying substrate, annealing temperature, film thickness, working pressure and substrate temperature. Although there were many publications on LSMO films grown on single crystal oxide substrates, like $SrTiO_3$ [7], $LaAlO_3$ [8], $NdGaO_3$, MgO [9], piezoelectric substrate [10] and silicon[6], still using of amorphous substrates such as glass are very limited[11]. In this paper, LSMO films were successfully grown directly on glass (Corning) substrates by PLD from a LSMO stoichiometric ceramic target in oxygen atmosphere. The crystal structures, surface morphology, resistivity, magneto-transport and the various interrelationships between these characteristics are discussed. Finally, the highest value of Curie temperature (T_C) as compared with literature for LSMO film deposited on low-cost amorphous glass substrate is reported.

2. MATERIALS AND METHODS

Bulk samples of $La_{5/8}Sr_{3/8}MnO_3$ as targets were prepared by the solid state reaction method. A well-mixed stoichiometric amount of high purity (>99.9%) powders of La_2O_3 , $SrCO_3$ and Mn_2O_3 were pre-sintered at $900^\circ C$ in air for 12h. After pre-sintering, the powders were ground and press into pellets of 13mm in diameter. Then the pellets were sintered at $1300^\circ C$ in air for 24h. The $La_{5/8}Sr_{3/8}MnO_3$ films were fabricated by pulsed laser deposition technique (Nd: YAG laser, $\lambda=532nm$). The films were grown directly on glass (Corning) under O_2 pressure of 12mtorr. The deposition temperature was $700^\circ C$. The thickness of film, $t \approx 237nm$ was determined using profilometry measurement. In order to avoid oxygen deficiency, a post-annealing at $700^\circ C$ for 4 h was made in air. The crystal structure of the films was characterized by X-ray diffraction measurement (XRD) and data were refined by the Rietveld method. The electrical transport properties were measured by the four-point method in the range of 100-300K. Magnetoresistance measurement (MR) was used to measure the change in resistance under an external applied magnetic field up to 1 Tesla with temperature ranging from 80 to 300K using Hall measurement system (model Lake Shore 7604). The AC Susceptibility measurements were performed using a CryoBINDT model. Finally, the surface morphology of the LCMO film was characterized by Field Emission - Scanning Microscope (FE-SEM).

3. RESULTS AND DISCUSSION

The X-ray diffraction (XRD) patterns of LSMO film and bulk were recorded at room temperature and are shown in Figure1. The XRD data were refined by the Rietveld method using the

X Pert HighScore Plus program. Figure 2 shows the results obtained for the Rietveld analysis of film sample. The selected refined data were listed in Table 1. The films showed the same structure as bulk, which is single phase rhombohedral with space group of $R\bar{3}C$. The average crystallite size and strain values have been calculated by using Williamson- Hall method [12]. The crystallite size (D) and lattice strain (ϵ) of thin film were 28.14 and 0.1139 respectively. The results are given in Table 1. One can see from Table.1 that lattice parameters and unit cell volume for thin film sample are compressed when compared with LSMO bulk. It may be due to lattice misfit between film and amorphous substrate. The major compounds in corning glass are SiO_2 , Al_2O_3 , B_2O_3 and CaO and their lattice parameters are all smaller than that of LSMO. Moreover, corning glass (Cg) is amorphous.

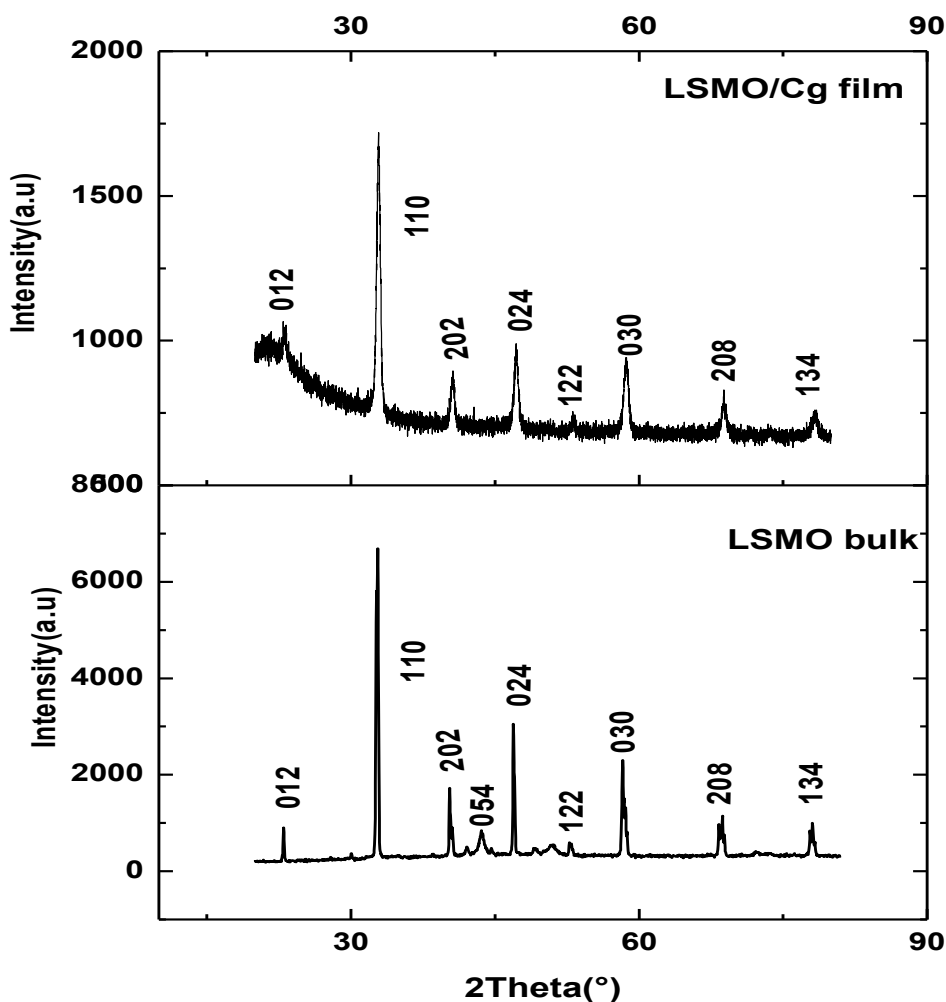


Figure 1. Room temperature XRD patterns of LSMO bulk and thin film.

Therefore, compressive strain exists inevitably in the films due to the lattice mismatch between the substrate and the LSMO. The Mn-O-Mn bond angle and Mn-O bond length obtained from the Rietveld refinement are presented in Table 1. As shown in table1 the Mn-O bond length is decreased for LSMO/Cg thin film as compared to the bulk sample. Hence, the Mn-O-Mn band angle is slightly

increased. It is well known, that changes in the Mn-O-Mn bond angle significantly influence the electrical properties of the samples.

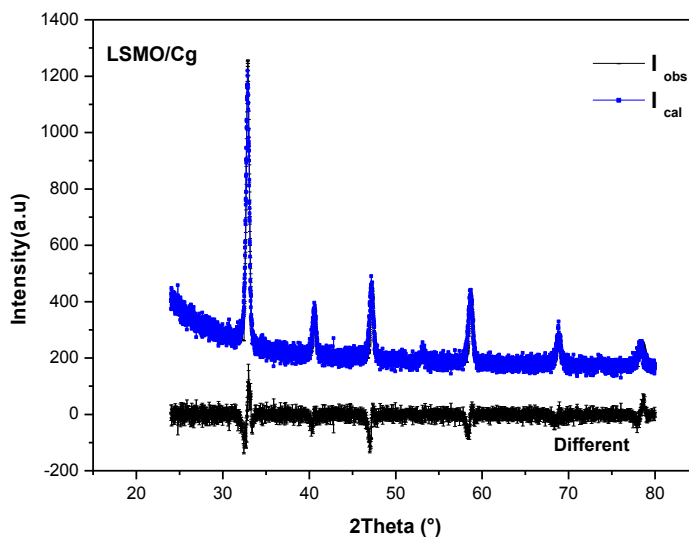


Figure 2. Rietveld analysis of XRD data for LSMO/Cg thin film.

Table 1. Structural parameters of LSMO bulk and thin film.

Structural Parameters	LSMO/Cg	LSMO(Bulk)
	Samples	
a(Å)	5.4648	5.4895
b(Å)	5.4648	5.4895
c(Å)	13.3165	13.3552
v(Å) ³	344.416	348.538
Lattice strain (%)	-0.1139	0.178
Cry.size(nm)	28.14	103.5
Mn-O(1)(Å)	1.940×6	1.948×6
Mn-O(1)-Mn(°)	167.710	167.703
R_{exp}(%)	6.0181	5.2783
R_{pr}(%)	8.6290	6.7636
R_{wpr}(%)	10.6939	8.4345
Goodness of fit	3.1578	2.5535

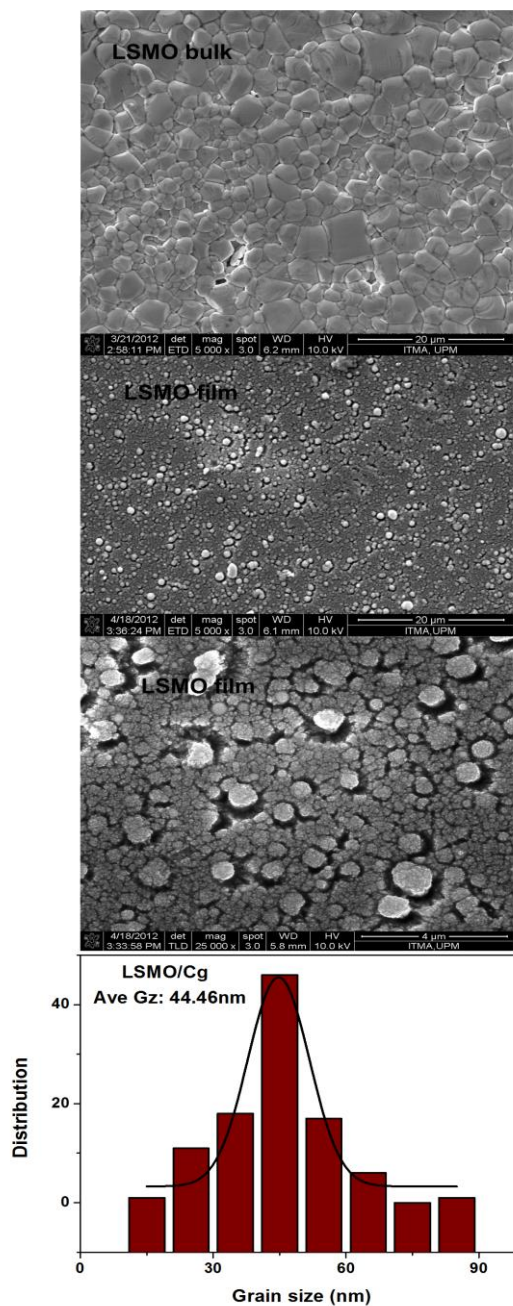


Figure 3. FE-SEM images and distribution of grain size of LSMO thin film.

The surface morphologies of the film and bulk are investigated by field emission- scanning electron microscopy (FE-SEM). Figure 3 shows the FE-SEM micrographs of film and bulk. The surface of film appears porous and cauliflower -like morphology follow island-like growth model. The average grain size of LSMO/Cg film is 44.46 nm. This value is much lower than that of the bulk as can see in Figure 1. The grain size distribution of film is analyzed based on 100 grains taken from SEM is shown in Figure1. A few scattered droplets are observed on top of film with average size of 3 μ m. This is quite common for PLD films growth, because of the pulsed laser ablates some boulders particles from the target, and some of boulders was transported through the shock wave in the laser plume, and deposited on the substrate [4].

Figure 4 shows normalized temperature dependent of the samples in zero magnetic fields in the temperature range of 100–300 K. Phase transition temperature (T_P) is higher than room temperature for both samples. For LSMO film deposited on glass substrate with $T_P > 300K$ is the highest metal-insulator transition temperature (T_{MI}), that is reported in literature for amorphous substrates[11, 13]. The resistivity of LSMO/Cg thin film is below 2 ($\Omega.cm$) that is lower than the resistivity of thin films as usual. In order to understand the conduction mechanism, the electrical resistivity data are fitted using the following equations [14-16]:

$$\rho = \rho_0 + \rho_2 T^2 \tag{1}$$

$$\rho = \rho_0 + \rho_{2.5} T^{2.5} \tag{2}$$

$$\rho = \rho_0 + \rho_2 T^2 + \rho_{4.5} T^{4.5} \tag{3}$$

Where ρ_0 is the temperature independent part that is due to the domain, grain boundary and other temperature independent mechanisms. The $\rho_2 T^2$ term corresponds to electron-electron scattering process and the $\rho_{2.5} T^{2.5}$ term arises due to electron-magnon scattering process and the $\rho_{4.5} T^{4.5}$ is a combination of electron-electron, electron-magnon and electron-phonon scattering process. The experimental data for thin film and bulk were fitted to the above equations. From the fitting results is found that the square of linear correlation coefficient R^2 for both samples is highest when the data are fitted by Eq. (3). Therefore, the electrical resistivity in the metallic region can be explained on the basis of electron-electron and electron-magnon (phonon) scattering mechanisms for the both film and bulk samples. Figure 5 is shown the ρ versus temperature for LSMO/Cg thin film below 300K that is fitted with Eq. (3). The resistivity parameters are obtained in Table 2. The value of the electron-electron scattering term ρ_2 , in Eq. (3) is larger than that of the electron-magnon (phonon) $\rho_{4.5}$ for film and bulk samples. Therefore, the electron-electron scattering displays a major role on conductivity of samples in metallic regime. On the other hand all resistivity parameters of film are higher than that of the bulk indicating more electron-scattering process occurred in the film, results to increasing of the resistivity of film as compared to bulk.

Table 2. The fit parameters obtained from experimental resistivity data in the ferromagnetic metallic region for LSMO thin film and bulk samples.

Sample	$\rho = \rho_0 + \rho_2 T^2$			$\rho = \rho_0 + \rho_{2.5} T^{2.5}$			$\rho = \rho_0 + \rho_2 T^2 + \rho_{4.5} T^{4.5}$			
	ρ_0 ($\Omega.cm$)	ρ_2 ($\Omega.cm.K^{-2}$)	R^2	ρ_0 ($\Omega.cm$)	$\rho_{2.5}$ ($\Omega.cm.K^{-2.5}$)	R^2	ρ_0 ($\Omega.cm$)	ρ_2 ($\Omega.cm.K^{-2}$)	$\rho_{4.5}$ ($\Omega.cm.K^{-4.5}$)	R^2
LSMO/Cg (film)	1.9611	7.79×10^{-6}	0.99058	2.0205	4.25×10^{-7}	0.97677	1.9146	1.01×10^{-5}	-1.4×10^{-12}	0.99707
LSMO (bulk)	1.56×10^{-3}	6.02×10^{-8}	0.99814	2.01×10^{-3}	3.29×10^{-9}	0.99265	1.50×10^{-3}	6.32×10^{-8}	-1.84×10^{-15}	0.99829

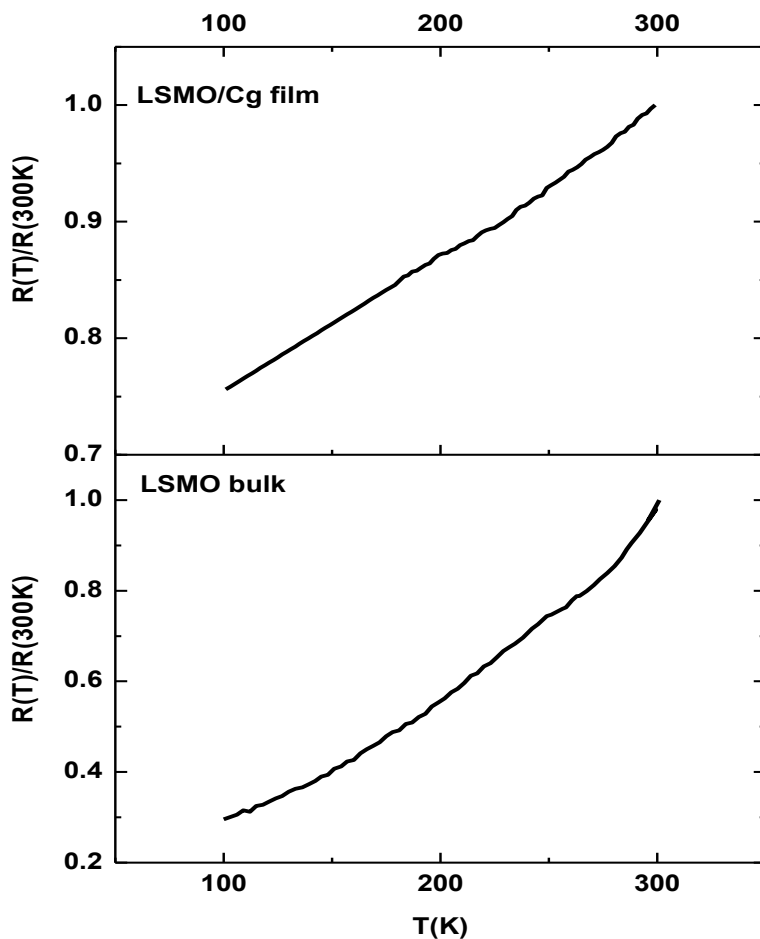


Figure 4. Normalized temperature dependent of the LSMO film and bulk in zero magnetic fields in the temperature range of 100–300 K.

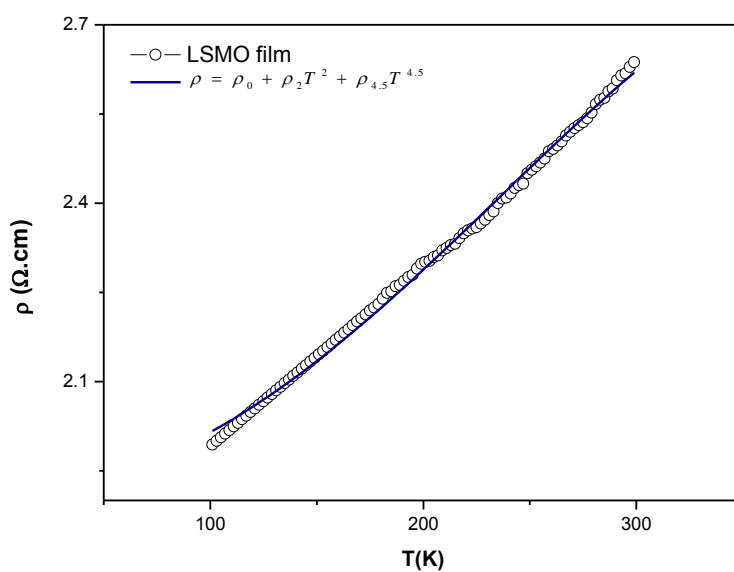


Figure 5. Resistivity vs. absolute temperature curve for LSMO /Cg thin film below T_P ; the solid line gives the best fit to Equation (3).

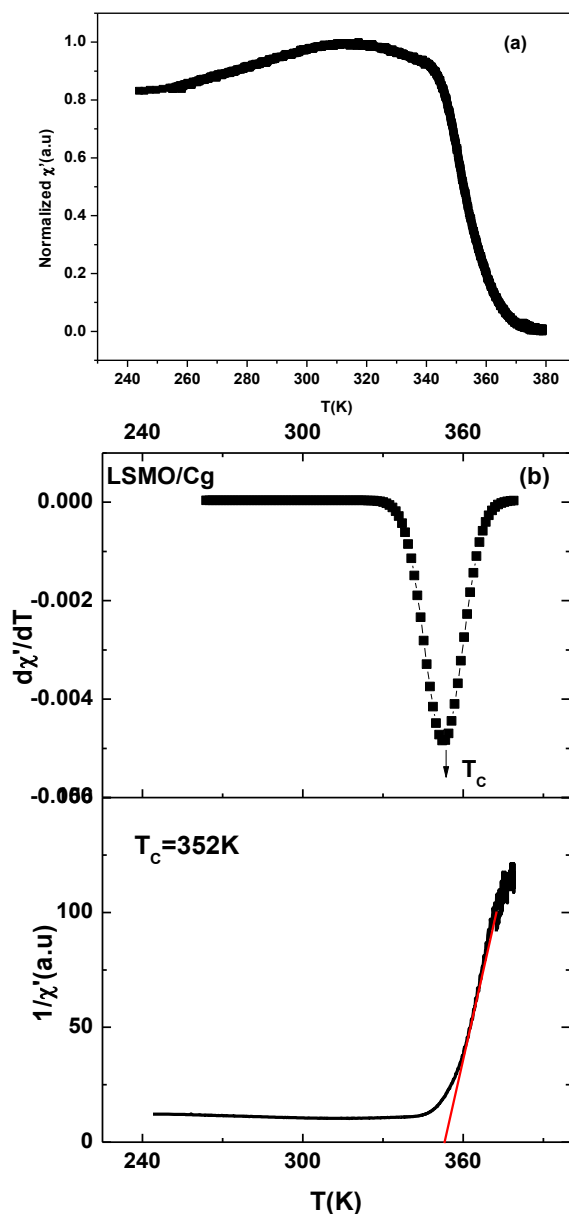


Figure 6. (a). Temperature dependence of real part of AC susceptibility for LSMO/Cg thin film in AC field amplitude of 1 Oe and frequency of 240 Hz; (b) T_c is found from the peak in the $d\chi'/dT$ via temperature curve or from inverse of susceptibility via temperature curve, where linear fit giving a Curie temperature .

Figure 6 shows the temperature dependence of real part of AC susceptibility for LSMO/Cg thin film in ac field amplitude of 1 Oe and frequency of 240 Hz. The thin film shows the paramagnetic to ferromagnetic transition at high temperature. The Curie temperature, T_c is found from the linear fit of inverse -susceptibility via temperature curve or from the peak in the $d\chi'/dT$ via temperature curve which are shown in figure 6(b). The T_c of LSMO/Cg thin film is 352K is the highest value that is reported in literature for amorphous substrates [11, 13] . The Curie temperature of LSMO/Cg film is higher than the bulk (331K) and is one of the highest in all reported of LSMO films deposited on various single

crystal substrates [11, 13, 17-19]. The high T_P , low resistance and high Curie temperature as high as 353K is proved the high quality of polycrystalline films is grown by PLD.

The %MR values versus applied magnetic field H at 1T, from 80K to 300K for all samples, are shown in Figure 2. The magnetoresistance ratio MR, is defined as $MR = 100 \times (R_H - R_0)/R_0$, where R_H and R_0 reflect the resistance measured with and without a magnetic field, respectively. Both film and bulk samples are shown negative MR values with a vertically applied magnetic field. The results showed that the resistivity decreases with increase in the magnetic field. The magnetoresistance could not reach saturation by an applied field of 1 T. Magnetoresistance (MR) of LSMO/Cg film is observed in a wide temperature range below the ferromagnetic transitions. The presence of low temperature MR, may be originating from spin-dependent scattering of polarized electrons at the grain boundaries. The highest MR value was -14.60% for film and -17.07% for bulk at 80K in a 1T magnetic field. One can see from SEM image that LSMO film has less grain boundary as compared with the bulk. Therefore, the film deposited on glass substrate displays lower MR as compared the LSMO bulk due to decreasing of spin polarization tunnelling that is induced by grain boundaries effect [20].

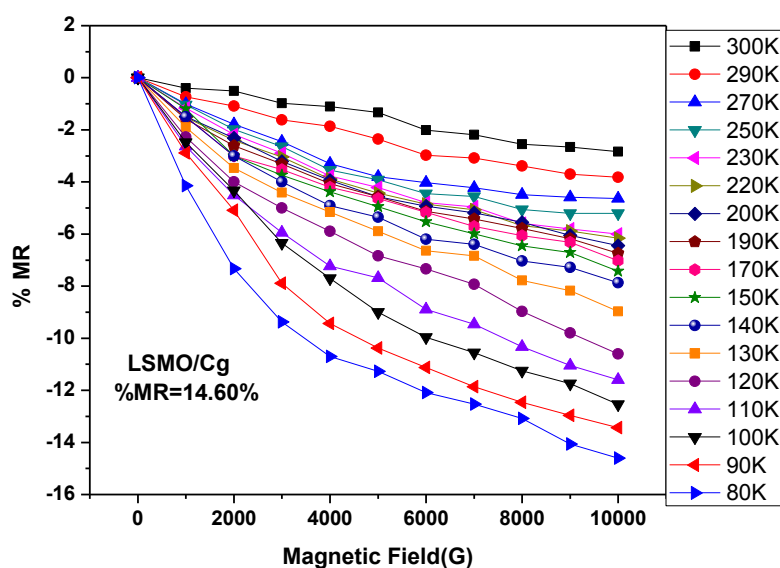


Figure 7. %MR curve of LSMO /Cg film as function of magnetic field at various temperatures.

4. CONCLUSIONS

In summary, LSMO films were successfully deposited on glass substrates without any additional buffer layer by Pulsed Laser Deposition. The structural characteristics, transport behaviors and magnetic properties of LSMO films were investigated. From the XRD pattern the film is found to be polycrystalline single-phases character. The LSMO top surface showed island growth and cauliflower-like morphology with average grain size of 44.46nm. The films exhibit a ferromagnetic transition at temperature (T_C) around 352 K, which is one on of the high in all LSMO films and as our knowledge, is the highest value that is reported in literature for amorphous substrates such as glass.

The metal-insulator transition temperature was above room temperature and electrical conduction mechanism of LSMO films at metallic regime, is due to the electron-electron (major) and electron-magnon scattering processes. The highest MR value of LSMO film was 14.60% at 80 K and 1 T. The low resistivity, high metal-insulator transition temperature, high T_C such as 352K makes these LSMO films very useful for room temperature magnetic devices.

ACKNOWLEDGEMENTS

The Ministry of Science, Technology and Innovation of Malaysia is gratefully acknowledged for the grant under Science Fund vote: 9199835.

References

- 1 S.S. Balevičius, V. ; Keršulis, S. ; Schneider, M. ; Liebfried, O. ; Plaušnaitienė, V. ; Abrutis, A., *IEEE Trans. Plasma Sci.*, 39 (2011) 411-416.
- 2 R. Von Helmolt, J. Wecker, B. Holzapfel, L. Schultz and K. Samwer, *Physical Review Letters*, 71 (1993) 2331-2333.
- 3 M.B. Salamon and M. Jaime, *Reviews of Modern Physics*, 73 (2001) 583-628.
- 4 W.L. Dan Liu *Ceramics International*, 37 (2011) 3531-3534.
- 5 D. Liu and W. Liu, *Ceramics International*, 38 (2012) 2579-2581.
- 6 D. Sahu, *Journal of Physics and Chemistry of Solids*, 73 (2012) 622-625.
- 7 S. Seo, H. Kang, H. Jang and D. Noh, *Physical Review B*, 71 (2005) 012412-012415.
- 8 T. Tsuchiya, K. Daoudi, T. Manabe, I. Yamaguchi and T. Kumagai, *Applied Surface Science*, 253 (2007) 6504-6507.
- 9 M. Spankova, S. Chromik, I. Vavra, K. Sedlackova, P. Lobotka, S. Lucas and S. Stancek, *Applied Surface Science*, 253 (2007) 7599-7603.
- 10 R. Gangineni, J. Kim, K. Nenkov and L. Schultz, *Journal of Magnetism and Magnetic Materials*, 324 (2012) 1153-1151.
- 11 Z.P. Shaojie Fang, Fenggong Wang, Liang Lin and Shenghao Han, *J. Mater. Sci. Technol*, 27 (2011) 223-226.
- 12 G. Williamson and W. Hall, *Acta Metallurgica*, 1 (1953) 22-31.
- 13 W.L.K. S.Y. Yang, Y. Liou, W.S. Tse, S.F. Lee, Y.D. Yao, *Journal of Magnetism and Magnetic Materials*, 268 (2004) 326-331.
- 14 A. Banerjee, S. Pal and B. Chaudhuri, *The Journal of Chemical Physics*, 115 (2001) 1550-1558.
- 15 L. Pi, L. Zheng and Y. Zhang, *Physical Review B*, 61 (2000) 8917-8921.
- 16 G.J. Snyder, R. Hiskes, S. DiCarolis, M.R. Beasley and T.H. Geballe, *Physical Review B*, 53 (1996) 14434.
- 17 S.C. M. S ˇpankova ´, I. Va ´vra , K. Sedla ´c ˇkova ´ , P. Lobotka , S. Lucas , S. Stanc ˇek *Applied Surface Science*, 253 (2007) 7599-7603.
- 18 D.R. Saha, *Journal of Alloys and Compounds*, 503 (2010) 163-169.
- 19 B.G.A. I.T.Gomes , A.M.L.Lopes , J.P.Arau ´ jo , J.Barbosa , J.A.Mendes, *Journal of Magnetism and Magnetic Materials*, 322 (2010) 1174-1177
- 20 S.Y. Pai Li, Li Liu, Xueli Wang, Yongqiang Wang, Zhaoming Tian, Jinghua He, and K.L. Shijun Yuan, Shiyang Ying, Chuanhui Wang, *Solid State Communications*, 146 (2008) 515-521.